Mineralium Deposita (1999) 34: 150 – 162

ARTICLE

Jiang Neng · Xu Jiuhua · Song Mianxin

Fluid inclusion characteristics of mesothermal gold deposits in the Xiaoqinling district, Shaanxi and Henan Provinces, People's Republic of China

Received: 15 May 1997 / Accepted: 10 June 1998

Abstract Fluid inclusions were studied in quartz samples from early (stage I) gold-poor quartz veins and later (stage II) gold- and sulphide-rich quartz veins from the Wenyu, Dongchuang, Qiangma, and Guijiayu mesothermal gold deposits in the Xiaoqinling district, China. Fluid inclusion petrography, microthermometry, and bulk gas analyses show remarkably consistent fluid composition in all studied deposits. Primary inclusions in quartz samples are dominated by mixed CO_2-H_2O inclusions, which have a wide range in CO_2 content and coexist with lesser primary CO_2-rich and aqueous inclusions. In addition, a few secondary aqueous inclusions are found along late-healed fractures. Microthermometry and bulk gas analyses suggest hydrothermal fluids with typically 15–30 mol% CO_2 in stage I inclusions and 10–20 mol% CO_2 in stage II inclusions. Estimates of fluid salinity decrease from 7.4–9.2 equivalent wt.% NaCl to 5.7–7.4 equivalent wt.% NaCl between stage I and II. Primary aqueous inclusions in both stages show consistent salinity with, but slightly lower Th_{total} than, their coexistent CO_2-H_2O inclusions. The coexisting CO_2-rich, CO_2-H_2O, and primary aqueous inclusions in both stage I and II quartz are interpreted to have been trapped during unmixing of a homogeneous CO_2-H_2O parent fluid. The homogenisation temperatures of the primary aqueous inclusions give an estimate of trapping temperature of the fluids. Trapping conditions are typically 300–370 °C and 2.2 kbar for stage I fluids and 250–320 °C and 1.6 kbar for stage II fluids. The CO_2-H_2O stage I and II fluids are probably from a magmatic source, most likely devolatilizing Cretaceous Yanshanian granitoids. The study demonstrates that gold is largely deposited as pressures and temperatures fall accompanying fluid immiscibility in stage II veins.

Editorial handling: R. Goldfarb

Jiang Neng[1] (✉)
Research Centre of Mineral Resources Exploration,
Chinese Academy of Sciences. PO Box 9701, Beijing 100101,
P R China
e-mail: jiangn@mail.c-geos.ac.cn

Present address:
[1]Institute of Geology, Chinese Academy of Sciences. PO Box 9825,
Beijing 100029, P R China

Xu Jiuhua
Department of Geology, Beijing University of Science
and Technology, Beijing, 100083, P R China

Song Mianxin
Department of Geology, China University of Geosciences,
Beijing, 100083, P R China

Introduction

The Xiaoqinling gold district is located along the border area of the Henan and Shaanxi provinces in east-central China (Fig. 1). It is the second largest gold producing district in China, with an estimated geological reserve of 380 metric tons of gold (Li et al. 1996). Five large (> 20 metric tons gold), 10 medium (> 5, < 20 metric tons gold), and more than 20 small (< 5 metric tons gold) lode gold deposits occur in the area. Unlike the mesothermal lode gold deposits in the Archean cratons of Western Australia and Canada, mineralisation and magmatism in the Precambrian basement rocks of the Xiaoqinling district are Jurassic to Cretaceous (Yanshanian orogeny), occurring about 2000 Ma after regional metamorphism of the basement rocks. The gold-bearing quartz veins contain abundant primary fluid inclusions, which are normally characterised by high CO_2 contents. Fluid inclusion studies on many individual gold deposits in the district have been carried out (Luan et al. 1985; Li et al. 1989; Ji 1991; Xie et al. 1996). However, these studies only reported ore fluid temperature, pressure and/or salinity. Furthermore, no distinction was made within these data those for primary versus secondary inclusions. In addition, little has been published about the fluid's composition, evolution, and association with gold deposition. One aim of this

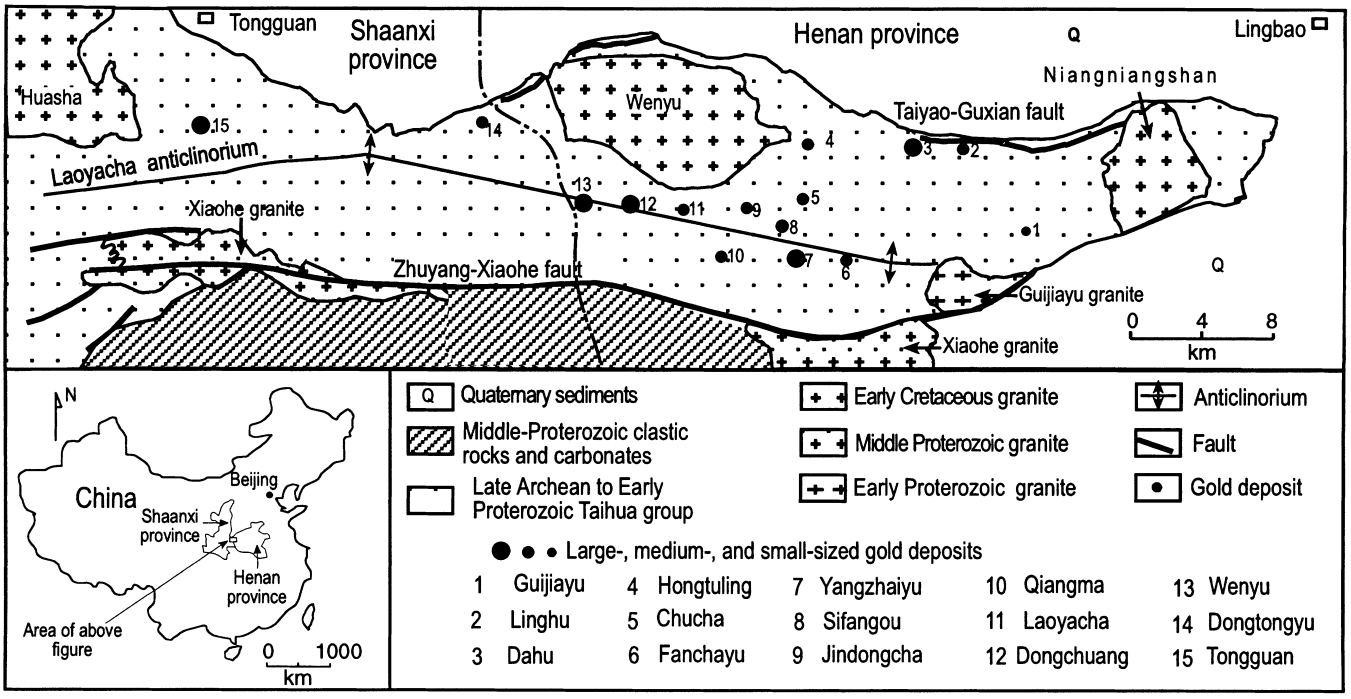

Fig. 1 General geology of the Xiaoqinling gold district (Modified from Luan et al. 1991). Most small gold deposits are not listed

work is to document the hydrothermal fluid evolution and to use this to determine possible mechanisms by which the gold was deposited. In addition, most auriferous quartz veins are approximately E-W trending, whereas a minority strike in other directions. Therefore, another goal is to compare the fluids in the different striking veins.

Four gold mines were chosen for this study. They are Wenyu, Dongchuang, Qiangma and Guijiayu mines. The first two are large deposits and dominated by E-W-striking veins, whereas the later two are dominated by N-S-striking veins and are medium and small deposits, respectively.

Geological setting

The Xiaoqinling gold district is located in a basement-cored uplift at the southern margin of the North China platform. According to Lin et al. (1989), the basement rocks in the area are those of the Late Archean to Early Proterozoic Taihua Group. They consist of amphibolite, biotite plagioclase gneiss, quartzite, and marble; were metamorphosed to amphibolite facies; and are of basic-igneous and semipelitic protolith character. Migmatization is widespread. The oldest and youngest isotopic ages from the Taihua Group are 2549 Ma and 1864 Ma as determined by Rb-Sr whole rock methods (Luan et al. 1991).

Repeated magmatism in the area is represented by the Songyangian Early Proterozoic Guijiayu biotite hornblende granite dated at 1748 Ma by Rb-Sr whole rock methods (Li et al.1996); the Jinningian Middle Proterozoic Xiaohe biotite granite with a U-Pb zircon date of 1463 Ma (Li et al.1996); and the Huashan, Wenyu, and Niangniangshan biotite granites with K-Ar biotite date of 108–130 Ma (Luan et al.1991). These latter dates reflect granite emplacement during the Yanshanian orogen. The depth of these Yanshanian granitoids is estimated to be 5 to 7 km (Luan et al. 1991). In addition, many diabase and lamprophyre dikes occur in the district. Most of these occur in E-W-striking directions but some are NE- and NW-striking. These dikes continue for up to 1 km along strike and range from 1 to 3 m in width. Field relations show that the diabase dikes are cut by auriferous veins and the latter are cut by lamprophyre dikes. The diabase and lamprophyre dikes were dated at 148–182 Ma and 76 Ma, respectively, using K-Ar methods on biotite (Chao 1989). Therefore, the ore-bearing veins were emplaced between 148 and 76 Ma. All gold-bearing quartz veins occur within 2 to 10 km of the three Yanshanian granitoid intrusions and are especially common in the vicinity of the Wenyu granitoid, suggesting a genetic link with the Yanshanian granitoids (Luan et al. 1985, 1991; Chao 1989; Li et al. 1989). However, neither quartz veins, nor the dikes, show any cross-cutting field relations with the three Yanshanian granitoids. More precise geochronological studies will be needed to define the exact age of the quartz veins and their temporal relationship with the Yanshanian granitoids.

Rocks of the Taihua group, all auriferous quartz veins, and the Cretaceous plutons are bounded by the Taiyao-Guxian fault in the north and by the Zhuyang-Xiaohe fault in the south. The east-west trending Laoyacha anticlinorium is found in the central portion of the area (Fig. 1). The gold occurrences are located along both limbs of this structure.

Gold-bearing veins

More than 1000 auriferous mesothermal-type quartz veins have been found in rocks of the Taihua Group in the Xiaoqinling area. The veins range from a few centimetres to over 8 m in thickness, up to 4.2 km along strike (505 vein, Wenyu mine and 60 vein, Yangzhaiyu mine) and up to hundreds of metres in vertical extent (e.g. 840 m in the Wenyu mine) (Li et al. 1996). Most veins, especially the larger ones in the district, strike E-W and form two groups dipping 25° to 45° north and 25° to 60° south. Other veins strike N-S, NE, and NW, with a variety of dips. Repeated pinching and swelling of the veins along strike is common. Ore shoots are preferentially located in swells resulting from a change in the strike and dip of the veins. The mineralised veins consist chiefly of quartz, lesser carbonate, pyrite, and base metal sulphides, and occasional magnetite and wolframite. The host rocks for the four studied

deposits are amphibolite, biotite plagioclase gneiss, and various migmatites. There are no significant differences in host rock types among the four deposits; all three host rock types are present at each deposit. Quartzite and marble, although regionally important, are never found to be host rocks.

The Wenyu mine is currently the largest producer in the Xiaoqinling district, with an annual production of about 1.5 metric tons of gold and an overall average grade of 10 g Au/metric ton. About 40 mineralised veins have been found at the Wenyu deposit. Most veins strike 90° to 120°, and dip 40° to 55° to the south. The veins can be traced for up to 4.2 km along strike and vary between 0.2 and 8.2 m in thickness. The Wenyu mine workings have been extended to a depth of greater than 400 m.

The Dongchuang mine was established in the 1980s with a geological reserve of 50 metric tons of gold. Up to the present time 19 mineralised veins have been found in the mine. All but one of these strike nearly E-W. The veins dip 34°–60°S and are typically 1- to 1.5-m-thick, although in some cases they extent to 13 m in thickness. Orebodies are normally 500–800 m in length and 500–800 m in vertical extent.

The Qiangma mine hosts the largest N-S striking vein in the district, number 410. It is 1680 m along strike, 0.2- to 5.9- m-wide and about 600 m in vertical extent. It dips 60°–80°E.

The Guijiayu mine is situated about 4 km west of the Niangniangshan granitoid. The veins there strike nearly N-S and dip 50°–60°W, are less than 500-m-long and are 0.1- to 1-m-thick.

Mineralogy and paragenesis

Mineralogy of the orebodies is simple and similar among the four studied deposits, although the proportions of minerals in the veins vary from one to another deposit. Pyrite and galena are abundant in the Wenyu and Dongchuang mines and they together make up 15–30% of the vein system. Other sulphides such as chalcopyrite and sphalerite each make up 2–3% of the veins. There is more galena at the Dongchuang mine, where the veins contain the highest content of galena in the whole district. At the Qiangma mine, the dominant sulphides are pyrite and chalcopyrite, which together make up 5 to 10% of the veins. Galena and sphalerite are minor. At the Guijiayu mine, only pyrite can reach 2 to 5% of the vein material. Other sulphides are minor. Nevertheless, the veining stages are the same among the four deposits. Three stages of veining have been identified on the basis of mineralogical, textural, and crosscutting relationships observed in hand specimens and thin sections. They include a pyrite-quartz stage (I), a quartz-sulphide stage (II) and a carbonate-quartz stage (III).

Stage I

Pyrite-quartz veins occur as fracture-fillings and form the main part of the vein systems, but only contain minor amounts of gold. In this stage, compact and massive milky white quartz is the most abundant mineral and composes more than 95% of the veins. Coarse-grained euhedral pyrite may comprise up to 5% of the veins. These early veins also contain minor amounts of magnetite and wolframite.

Stage II

Quartz-sulphide veins, which contain abundant sulphides and economic amounts of gold, often cut stage I veins. In some cases, they occur along both margins of stage I veins. Smoky anhedral quartz comprises 40–50% of the veins and sulphide minerals, including pyrite, chalcopyrite, galena, and sphalerite, comprise 50–60%. Pyrite is typically subeuhedral to anhedral and fine-grained (normally 0.2–2 mm in diameter).

In some veins, such as the 530 vein in the Wenyu mine, stage II mineralisation is divisible into two substages: IIa, during which smoky anhedral quartz, pyrite and chalcopyrite were deposited; and IIb, which is marked by deposition of translucent to transparent vuggy quartz and large amounts of euhedral pyrite and galena together with fine-grained anhedral chalcopyrite and sphalerite. Galena is typically sub- to euhedral and ranges from 0.2 to 4 mm in diameter. Chalcopyrite and sphalerite are usually anhedral and range from 0.2 to 2 mm in diameter.

Stage III

Stage III carbonate-quartz veins consist of dominantly calcite and/or dolomite. The veins are normally less than 1 cm in width, and crosscut stage I and II veins. Calcite and/or dolomite comprise between 80 and 90% of the veins. Grey chalcedonic quartz comprises from 10 to 20% of the veins. Medium- to fine-grained euhedral pyrite may comprise up to 1% of the veins.

Gold occurrence

The occurrences of gold in the deposits of the Xiaoqinling district have been well documented by Fang (1985a, b) and Luan et al. (1985), and are here integrated with our own microscopic studies. Most gold exists as native gold in pyrite. Small amounts of gold exist as electrum and rarely as gold-tellurides. Native gold contains between 0.83 and 19.20% silver, although typically between 3 and 7%. Electrum contains 69.5 to 74.2% gold. Gold-tellurides contain 22.5 to 34.5% gold, 4.1 to 9.8% silver and 57.1 to 72.2% tellurium. Gold and electrum mainly occur in sulphides, especially in pyrite. A small amount of gold also occurs in chalcopyrite, galena and sphalerite or as free gold in quartz. Gold grades usually increase where pyrite is most abundant.

Because over 90% of gold in gold-bearing veins occurs in pyrite (e.g. about 94% of the gold is in pyrite in the 505 vein of the Wenyu mine, and about 93% of the gold is in pyrite in the 60 vein of the Yangzhaiyu mine), we assume that the gold content of pyrite from the different paragenetic stages represents relative gold abundance of each stage. Among pyrite of all three stages, pyrite of stage II contains the highest content of gold,

ranging from 6.6 to 1200 ppm ($n = 57$). Whereas coarse-grained euhedral pyrite in stage I veins contains 0.19–136 ppm ($n = 15$) and fine-grained euhedral pyrite in stage III veins contains the lowest content of gold, only 3.6–39.6 ppm ($n = 8$). In pyrite of stage I and III, gold generally occurs as inclusions. In pyrite of stage II, gold occurs as inclusions, and as fracture-fillings with sulphide grains, and as blebs that coexist with adjacent anhedral chalcopyrite and galena.

Alteration

Wall-rock alteration extends for up to several metres from vein margins and develops secondary mineral assemblages of quartz, sericite, carbonate, K-feldspar, epidote, and chlorite with the abundances of these minerals varying with different wall rock types. For example, K-feldspar is more common in silica-rich rocks such as the various migmatites, whereas chlorite is more abundant in more basic rocks such as amphibolite and biotite plagioclase gneiss.

Two alteration zones are identified around the veins, going from unaltered rocks toward the veins: (1) an outer epidote-carbonate-chlorite zone in basic host rocks, or a K-feldspar-quartz-sericite zone in relative more felsic host rocks; (2) an inner quartz-sericite zone in both basic and felsic host rocks. Contacts between the two alteration zones are generally gradational.

K-feldspar and epidote are the earliest formed alteration minerals, which replace plagioclase and hornblende and are later replaced by sericite and chlorite, respectively. In addition, plagioclase and hornblende can also be replaced by sericite and chlorite, respectively. Biotite is replaced by chlorite. Earlier carbonates are associated with sericite which replaces K-feldspar. Later carbonates are coeval with quartz and fill fractures. Quartz is common throughout the alteration sequence. The chronology of alteration minerals is generally determined by pseudomorphic replacement. The alteration minerals related to stage I are chiefly K-feldspar, epidote and quartz, with minor sericite and chlorite. The alteration minerals related to stage II are chiefly quartz, sericite and chlorite, with minor carbonates. Alteration associated with stage III is weak and the associated mineral phases are solely quartz and carbonates.

Fluid inclusion petrography

Quartz-sulphide material from each vein stage at the Wenyu, Dongchuang, Qiangma, and Guijiayu deposits was sampled for fluid inclusion analysis. Although the quartz itself contains only a very small amount of gold, and fluid inclusions and gold have not been found in physical contact, the quartz examined in this study is intimately intergrown with auriferous pyrite and/or other sulphides. Therefore, we assume that such quartz was deposited in the same mineralisation event as the pyrite that is interpreted as coeval with the gold.

Doubly polished sections were prepared for fluid inclusion petrography and microthermometry. Fluid inclusion observations were carried out from quartz of all three stages from the four mines. Unfortunately, no suitable fluid inclusions were found in quartz from the stage III carbonate-quartz veins. Fluid inclusions in quartz samples from stage I and stage II veins from the four investigated gold deposits can be divided into three compositional types: mixed CO_2-H_2O, CO_2-rich, and aqueous inclusions, by order of decreasing abundance. The various types of inclusions could be distinguished on the basis of their appearance at room temperature, combined with their cooling behaviour (down to –40 °C) and low temperature heating (up to about 31 °C). The CO_2-rich inclusions are defined by their lack of clathrate formation during cooling. Isolated inclusions, those forming irregular three-dimensional groups within grains, or those along growth planes were classified as primary (Roedder 1984). Inclusions occurring along planes cross-cutting grain boundaries were considered secondary inclusions (Roedder 1984)

CO_2-H_2O inclusions

CO_2-H_2O inclusions vary from 3 to 30 μm in diameter and average about 8 to 12 μm. They are the most abundant among the three types of inclusions, making up more than 90% of the primary inclusions. CO_2-H_2O inclusions may have irregular or negative crystal shapes and consist of two (liquid water + liquid CO_2) or three (liquid water + liquid CO_2 + CO_2-rich vapour) phases at room temperature. They occur as irregular, three-dimensional clusters or as trails but generally confined to individual quartz grains (Fig. 2A). They are thus considered as primary and pseudosecondary in origin.

In stage I quartz, the CO_2-H_2O inclusions usually have two phases at room temperature and their CO_2 volumetric proportion ranges from 20 to 80%, with an appreciable number of the inclusions containing 40 to 70 volume % CO_2 (Fig. 2B). In stage II quartz, the CO_2-H_2O inclusions typically have three phases at room temperature and their CO_2 volumetric proportion ranges from 10 to 80%, with most between 20 to 50 vol% CO_2 (Fig. 2C).

CO_2-rich inclusions

CO_2-rich inclusions are quite similar in size and distribution in quartz of both stage I and stage II. These inclusions, ranging from 3 to 8 μm, consist of a single or two (liquid CO_2 + vapour CO_2) phases at room temperature. No visible liquid water was found in the inclusions. The inclusions commonly exihibit negative crystal shapes (Fig. 2D) and are distributed within CO_2-

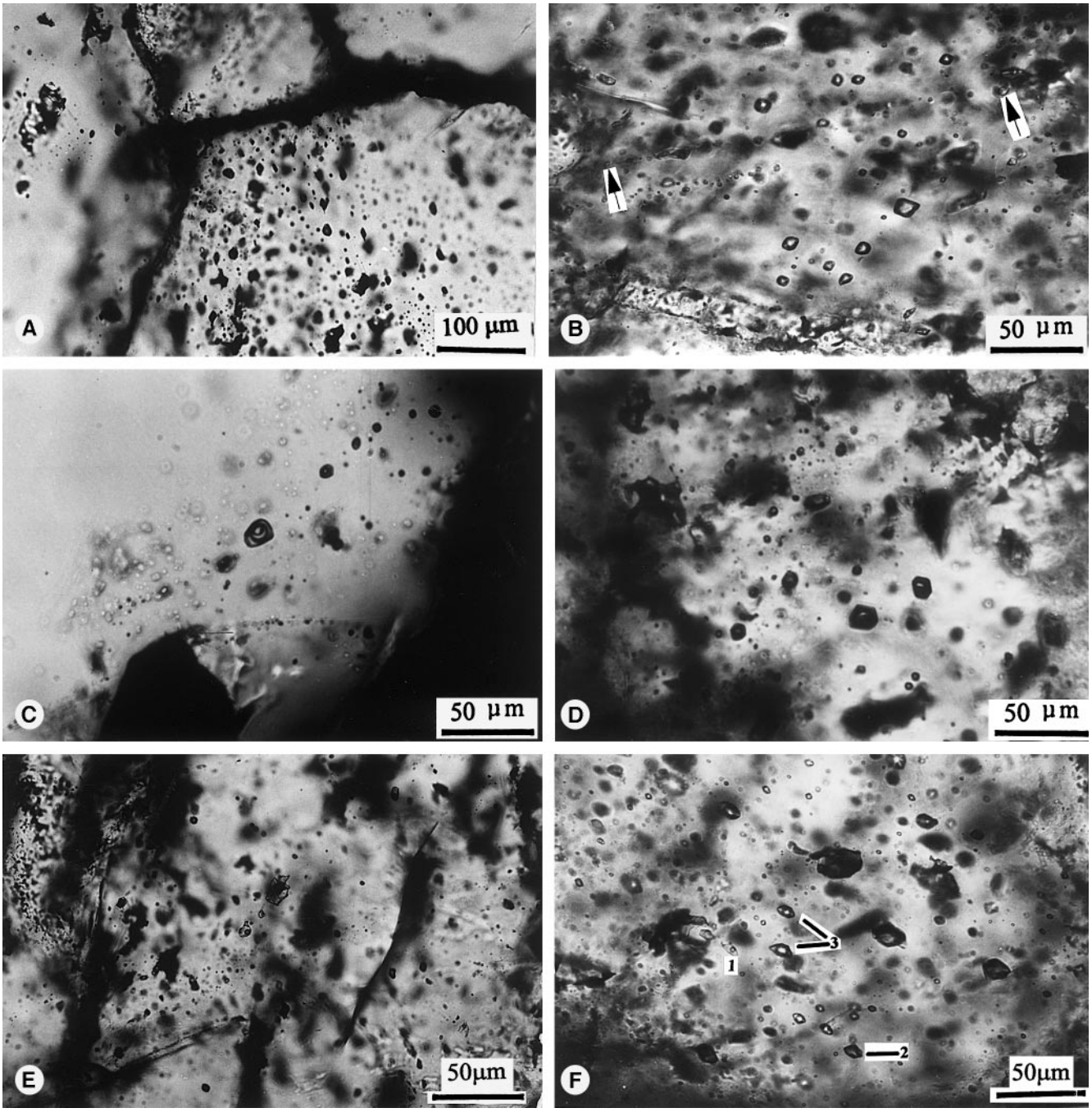

H_2O inclusions clusters. They are also considered primary in origin.

Aqueous inclusions

Aqueous inclusions occur in three different orientations in quartz of both stage I and stage II: as trails along healed fractures (Fig. 2B), as isolated inclusions (Fig. 2E) and coexisting with CO_2-H_2O inclusions (Fig. 2F). They all consist of two phases. Aqueous inclusions along healed fractures that cut across different quartz grains are common and range from 1 to 10 μm in

Fig. 2 A–F Photomicrographs of fluid inclusions from Xiaoqinling district showing the wide range of compositions of coexisting inclusions. **A** Irregular, three-dimensional cluster of CO_2-H_2O inclusions confined to quartz grains. **B** Two-phase CO_2-H_2O inclusions with more than 70 vol% CO_2 in stage I quartz. Small amounts of liquid water can be observed at the tips of inclusion walls intersecting at acute angles. At the top are CO_2-rich inclusions (slightly out of focus). *Arrows* refer to trail of smaller secondary aqueous inclusions. **C** Three-phase CO_2-H_2O inclusions with less than 50 vol% CO_2 typically in stage II quartz. **D** One-phase CO_2-rich inclusions with negative crystal shapes. **E** Isolated irregular aqueous inclusions. **F** Coexisting aqueous, CO_2-rich and CO_2-H_2O inclusions. *1*, Aqueous inclusions; *2*, one-phase CO_2-rich inclusion; *3*, two-phase (L_{H_2O} + L_{CO_2}) CO_2-H_2O inclusions

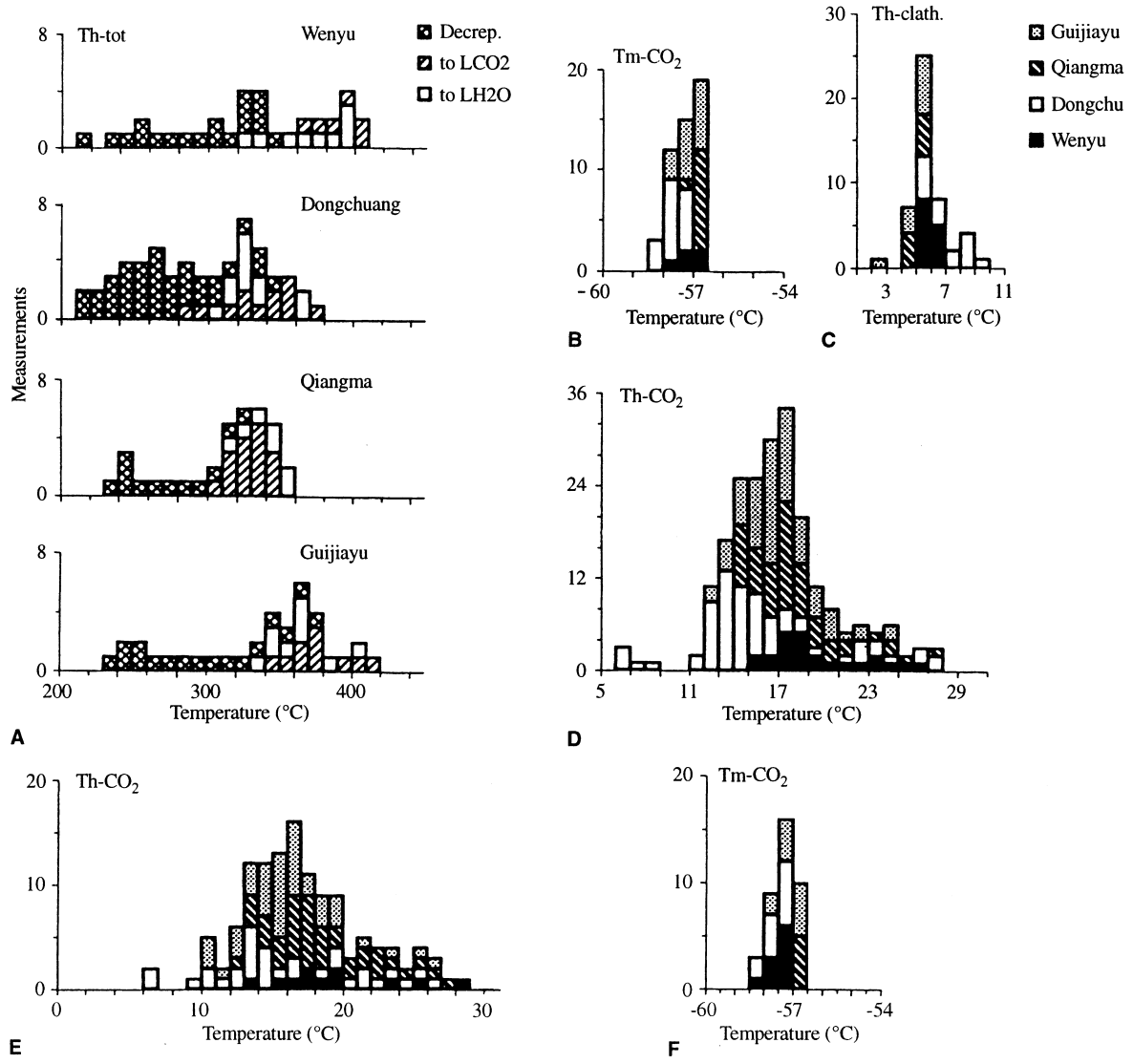

Fig. 3 A–I Microthermometric data for inclusions in quartz of stage I. **A–D** data for CO_2-H_2O inclusions, **E–F** data for CO_2-rich inclusions, **G–I** data for aqueous inclusions. In **B** and **D–E** the symbols used have the same meaning as in **C**. **G** *Th* of primary and secondary aqueous inclusions. **H** *Tm*-ice of primary aqueous inclusions. **I** *Tm*-ice of secondary aqueous inclusions. Symbols in **H** and **I** as in **C**

diameter with an average of 3 to 5 μm, and typically have irregular shapes. They are undoubtedly secondary in origin. Aqueous inclusions occurring as isolated inclusions or coexisting with CO_2-H_2O inclusions are rare and have irregular or round shapes. They range from 2 to 18 μm in diameter and are interpreted as primary in origin.

Fluid inclusion microthermometry

Microthermometric analyses were made using a Linkam TH600 heating-freezing stage attached to a Leitz Ortholux transmitted light microscope. The stage was calibrated using synthetic fluid inclusions. Estimated accuracy was ±0.1 °C at temperatures below 30 °C and ±1 °C at temperatures above 30 °C. Freezing experiments were performed first on all sections to avoid the decrepitation of inclusions. Resulting melting measurements included the final melting temperatures of ice (Tm_{ice}) and clathrate ($Tm_{clathrate}$) to determine fluid salinities. The melting temperature of CO_2 ($Tmco_2$) was also measured to evaluate the purity of the CO_2 phase. During heating of the fluid inclusions, attempts were made to measure the homogenisation temperature of the CO_2 ($Thco_2$), to determine the density of CO_2, and the total homogenisation temperature (Th_{total}).

Previous fluid inclusion measurements on two deposits of this study have been made by Luan et al. (1985), Li et al. (1989), Ji (1991) and Xie et al. (1996). Luan et al. (1985) reported a final Th_{total} of 200–340 °C for all inclusion types at the Wenyu mine, 126–336 °C at the Qiangma mine, and formation pressures of 1.48–1.63 kbar for stage I mineralisation and 1.08–1.27 kbar for stage II mineralisation in the whole district. Formation pressures of CO_2-H_2O inclusions given by

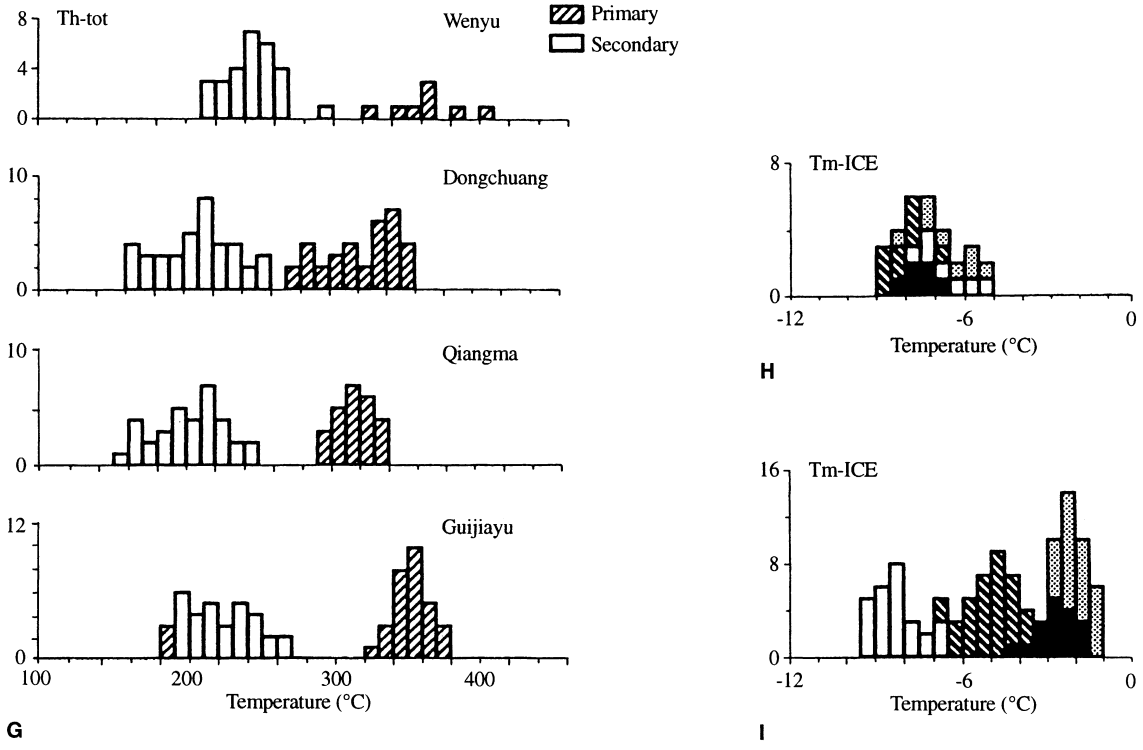

Fig. 3 (Contd)

Li et al. (1989) are 1.90–2.25 kbar for stage I and 1.25–1.80 kbar for stage II. Ji (1991) reported an average Th_{total} of 306 °C for stage I inclusions and 246 °C for stage II inclusions for the Wenyu mine. Xie et al. (1996) described both Th_{total} and salinity for CO_2-H_2O inclusions at the Wenyu and Qiangma mines (Wenyu mine, 291–306 °C for stage I and 260–277 °C for stage II, and an average salinity of 7.0–7.4 equivalent wt.% NaCl for both stages; Qiangma mine, Th_{total} of 289–356 °C for stage I and 210–272 °C for stage II, and an average salinity of 7.8–10.0 equivalent wt.% NaCl for both stages). They also described Th_{total} range of 145–162 °C for secondary aqueous inclusions at the Qiangma mine. Microthermometric data on CO_2-H_2O inclusions from other deposits in the Xiaoqinling district, such as the Tongguan mine, the Dongtongyu mine the Jindongcha mine, and the Yangzhaiyu mine, all fall in the Th_{total} range of 280–365 °C for stage I CO_2-H_2O inclusions and 240–290 °C for stage II CO_2-H_2O inclusions, and salinity range of 5.7–13.1 equivalent wt.% NaCl for all CO_2-H_2O inclusions of both stages (Xie et al. 1996).

Many of the larger CO_2-H_2O inclusions decrepitate before total homogenisation, especially those in stage I quartz where most inclusions have CO_2 volumetric proportions over 50%. However, arduous efforts were made to study small inclusions during heating experiments, and a number of reliable measurements for Th_{total} of CO_2-H_2O inclusions were recorded. They show a good reproducibility when replicate measurements were made during subsequent heating cycles. The homogenisation is either by CO_2 bubble expansion for inclusions with relatively high CO_2 contents or by CO_2 bubble shrinkage for inclusions with lesser amounts of CO_2. The former case most commonly characterises CO_2-H_2O inclusions in stage I quartz and the latter case is common of such inclusions in stage II quartz.

Inclusions in stage I veins

The CO_2-H_2O inclusions in stage I quartz homogenise between 281 °C and 412 °C (Wenyu mine, 324–408 °C; Dongchuang mine, 281–374 °C; Qiangma mine, 300–355 °C; Guijiayu mine, 337–412 °C) (Fig. 3A). Tm_{CO_2} of CO_2-H_2O inclusions from all four mines are quite similar, ranging from −56.5 °C to −58.2 °C (Fig. 3B), indicating probable presence of small concentrations of other gases (Shepherd et al.1985). Melting of clathrate was observed in most CO_2-H_2O inclusions between 2.9 °C and 9.1 °C, with a mode between 5.0 °C and 6.0 °C (Fig. 3C). Based on Collins (1979), these define a salinity range from 1.8 to 12.1 equivalent wt.% NaCl, with most values between 7.4 and 9.2 equivalent wt.% NaCl. All CO_2-H_2O inclusions from stage I quartz show that CO_2 homogenise, to a liquid. The Th_{CO_2} varies slightly among the four mines, with most measurements between 14–18 °C (Fig. 3D).

As shown in Fig. 3E and 3F, homogenisation and melting temperatures of CO_2 in the CO_2-rich inclusions are almost the same as those of CO_2-H_2O inclusions in stage I quartz. No clathrate formation was noted when freezing the CO_2-rich inclusions and no melting of such compounds was observed during subsequent heating.

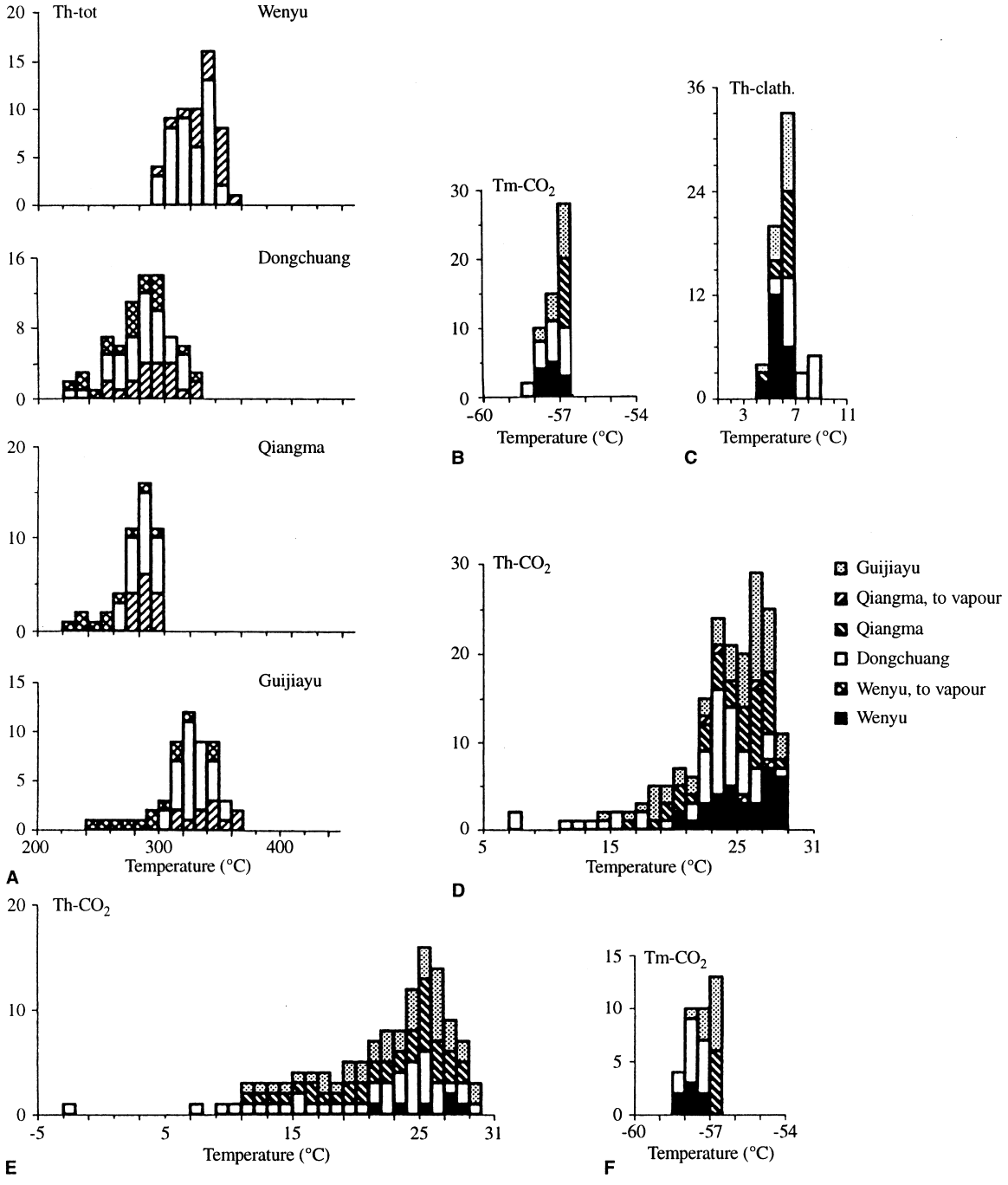

Fig. 4 **A–I** Microthermometric data for inclusions in quartz of stage II. **A–D** data for CO_2-H_2O inclusions, **E–F** data for CO_2-rich inclusions, **G–I** data for aqueous inclusions. Symbols in **A** same as in Fig. 3A. Symbols in **B** to **I** as in Fig. 3C. In the $Thco_2$ histogram, *to vapour* refers to homogenisation to vapour. **G** *Th* of primary and secondary aqueous inclusions; **H** *Tm*-ice of primary aqueous inclusions; **I** *Tm*-ice of secondary aqueous inclusions

Aqueous inclusions all homogenise into the liquid phase. The Th_{total} of aqueous inclusions in stage I quartz is distinguished by two distinct groups in all four mines (Fig. 3G). The higher temperature peak corresponds to primary aqueous inclusions (Wenyu mine, 322–403 °C; Dongchuang mine, 274–358 °C; Qiangma mine, 296–334 °C; Guijiayu mine, 324–377 °C), whereas the lower temperature peak corresponds to secondary aqueous inclusions (Wenyu mine, 215–291 °C; Dongchuang mine, 167–256 °C; Qiangma mine, 157–247 °C; Guijiayu mine, 181–265 °C). The small size of these aqueous inclusions limits the number of reliable observations on freezing behaviour. The Tm_{ice} of aqueous inclusions range from −5.1 °C to −8.8 °C for primary aqueous inclusions (Fig. 3H) and −1.3 °C to −9.3 °C for secondary ones (Fig. 3I). Using relationships in Bodnar (1993), the salinities range from 8.0 to 12.6 equivalent wt.% NaCl for primary aqueous inclusions and from 2.2 to 13.2 equivalent wt.% NaCl for secondary aqueous

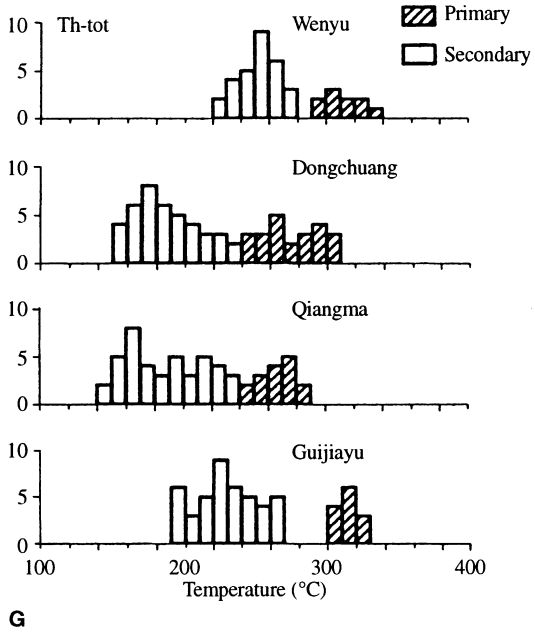

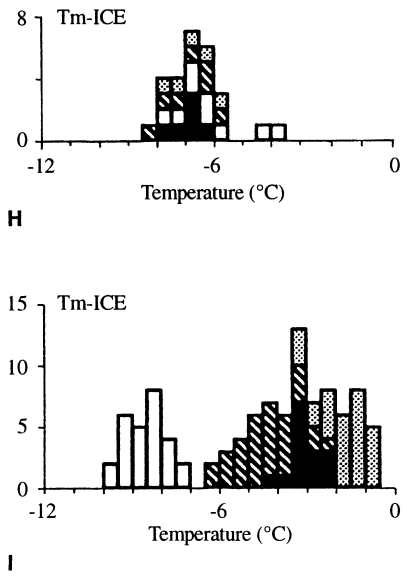

Fig. 4 (Contd)

inclusions. Because the primary aqueous inclusions are often coexistent with CO_2-H_2O inclusions, we assume that these inclusions may commonly be relatively low-gas end-member compositions. Owing to their small size, it is difficult to see clathrate behaviour during microthermometric experiments. Hence, the salinities based on ice melting could be maximum values and not the true values, if clathrate compounds are present.

Inclusions in stage II veins

The Th_{total} of CO_2-H_2O inclusions in stage II quartz range from 227 °C to 362 °C (Wenyu mine, 290–355 °C; Dongchuang mine, 227–323 °C; Qiangma mine, 268–298 °C; Guijiayu mine, 308–362 °C) (Fig. 4A). The $Tmco_2$ of CO_2-H_2O inclusions in stage II quartz from all four mines are quite similar to those from stage I quartz, ranging from −56.6 °C to −58.4 °C (Fig. 4B). The $Tm_{clathrate}$ of CO_2-H_2O inclusions range from 4.4 °C to 8.5 °C, with most between 6.0 °C and 7.0 °C (Fig. 4C). They correspond to a salinity range between 3.0 to 10.0 equivalent wt.% NaCl, with most between 5.7 and 7.4 equivalent wt.% NaCl. In all but two CO_2-H_2O inclusions from the Wenyu mine and three from the Qiangma mine, homogenisation of CO_2 occurred to the liquid phase. The $Thco_2$ of CO_2-H_2O inclusions in stage II quartz range from 7.1 °C to 28.9 °C, with most between 22 ° and 29 °C (Fig. 4D)

$Thco_2$ of CO_2-rich inclusions have the same range as those of CO_2-H_2O inclusions in stage II, with the exception that one CO_2-rich inclusion from the Dongchuang mine homogenises below 0 °C (Fig. 4E). Similarly, $Tmco_2$ of CO_2-rich inclusions show the same range as those of CO_2-H_2O inclusions in stage II quartz (Fig. 4F).

All aqueous inclusions also homogenise into the liquid phase in stage II quartz and define two distinct groups of inclusions (Fig. 4G). The higher temperature peak corresponds to primary aqueous inclusions (Wenyu mine, 290–335 °C; Dongchuang mine, 242–308 °C; Qiangma mine, 245–289 °C; Guijiayu mine, 306–328 °C), whereas the lower temperature peak corresponds to secondary aqueous inclusions (Wenyu mine, 226–279 °C; Dongchuang mine, 156–238 °C; Qiangma mine, 145–238 °C; Guijiayu mine, 194–267 °C). The *Tm*ice of aqueous inclusions range from −3.6 °C to −8.4 °C for primary aqueous inclusions (Fig. 4H), with a corresponding salinity of 5.9–12.2 equivalent wt.% NaCl. Measurements of −0.8 °C to −9.6 °C for the secondary inclusions (Fig. 4I) correspond to salinities of 1.4–13.5 equivalent wt.% NaCl.

Summary

The microthermometric data presented indicate that fluids trapped in quartz from the four studied deposits have many features in common. Firstly, the fluid types are the same, with CO_2-H_2O, CO_2-rich, and primary and secondary aqueous inclusions consistently observed from all four deposits. Secondly, CO_2-H_2O inclusions in stage I quartz have higher Th_{total}, salinity and CO_2 volumetric proportion, but lower $Thco_2$ than those in stage II quartz. Thirdly, the range of $Thco_2$ in both CO_2-rich and CO_2-H_2O inclusions is the same in a given sample. Fourthly, the range of salinity of CO_2-H_2O inclusions in stage I quartz is slightly wider than in stage II quartz. Finally, aqueous inclusions coexisting with CO_2-H_2O inclusions show slightly lower Th_{total} but higher salinity than CO_2-H_2O inclusions.

However, there are some differences in fluid characteristics among the four deposits. First, the average

Th_{total} of inclusions from the four deposits are somewhat different. The Wenyu and Guijiayu mines have slightly higher Th_{total} for both CO_2-H_2O and primary aqueous inclusions than do the Dongchuang and Qiangma mines. Similarly, Th_{total} of secondary aqueous inclusions from the Wenyu and Guijiayu mines are higher than from the Dongchuang and Qiangma mines. Second, the ranges of salinity, Th_{total} and/or $Thco_2$ for CO_2-rich and CO_2-H_2O inclusions are slightly different among the four deposits. The Dongchuang mine has the widest ranges of salinity (Dongchuang mine, 2.2 to 9.0 equivalent wt.% NaCl for stage I and 3.3 to 7.8 equivalent wt.% NaCl for stage II; Wenyu mine, 6.9 to 9.3 equivalent wt.% NaCl for for stage I and 6.6–7.6 equivalent wt.% NaCl for stage II; Qiangma mine, 6.9 to 9.6 equivalent wt.% NaCl for stage I and 6.9 to 9.3 equivalent wt.% NaCl for stage II ; Guijiayu mine, 7.8 to 12.1 equivalent wt.% NaCl for stage I and 7.4 to 10.0 equivalent wt.% NaCl for stage II), Th_{total} and/or $Thco_2$ for CO_2-H_2O inclusions and/or CO_2-rich inclusions in both stage I and II quartz.

Bulk inclusion gas analyses

Analytical method

Quartz was crushed to 2- to 4-mm-diameter grains, hand-picked, then ground to 40–80 mesh. Afterwards, the quartz samples were treated with distilled water (to dissolve salts) and aqua regia (to dissolve carbonates and sulphides). After each step, the reagent was decanted and the sample washed several times with double distilled water.

Approximately 0.25 g of cleaned quartz was heated to 550 °C (it was found that heating to that temperature caused thermal decrepitation of most of the inclusions) in helium after atmospheric gases were purged from the sample chamber. The released gases were then introduced into a gas chromatograph using a helium carrier gas flow. A standard gas mixture of known composition was used for calibration.

Results

Gas analyses were performed on some of the same samples which had been used for microthermometry. The composition of the released gases are given in Table 1.

On the whole, and consistent with the microthermometry, the inclusion fluids are composed chiefly of H_2O and CO_2. In all four mines, the CO_2 content in stage I quartz is much higher than that in stage II quartz. This accords well with the microscopic observations that most CO_2-H_2O inclusions have a CO_2 volumetric proportion of more than 50% in stage I quartz, whereas it is less than 50% in stage II quartz. The released gases generally contain between 23 and 56 mol% CO_2 in stage I quartz, in contrast to between 14 and 21 mol% CO_2 in stage II quartz.

Discussion

Fluid immiscibility

As described earlier, the primary aqueous, CO_2-rich and CO_2-H_2O inclusions coexist in a given inclusion cluster in quartz of both stage I and II. The aqueous and CO_2-rich inclusions are therefore interpreted to be the results of selective entrapment of unmixed aqueous and CO_2 compositions from a homogenous, one-phase CO_2-H_2O fluid. The wide variation of the CO_2 content in the CO_2-H_2O inclusions can be explained by mixed entrapment of the two end-members.

More evidence for fluid immiscibility comes from the pattern of homogenisation temperatures. First, the CO_2-H_2O inclusions have the same Th_{total} range, irregardless of whether they homogenise by CO_2 bubble shrinkage or

Table 1 Composition of fluid inclusion gases from quartz

Sample number	Sampling position	H_2O	CO_2	CO	CH_4	H_2O	CO_2	CO	CH_4
		(10^{-6} mol)				mol %			
W-5	Wenyu mine(I)	30.63	13.61	0.026	0.283	68.75	30.56	0.06	0.64
W-17	Wenyu mine(I)	5.50	7.00	–	–	44.00	56.00	–	–
W-6	Wenyu mine(II)	30.72	6.23	0.019	0.148	82.77	16.78	0.05	0.40
W-9	Wenyu mine(II)	12.3	2.83	–	0.043	81.07	18.65	–	0.28
DC-9	Dongchuang mine(I)	72.5	21.70	0.03	0.059	76.89	23.02	0.03	0.06
DC-17	Dongchuang mine(I)	25.76	20.60	0.015	0.232	55.27	44.20	0.03	0.50
DC-10	Dongchuang mine(II)	49.61	13.33	0.025	0.025	78.76	21.16	0.04	0.04
DC-21	Dongchuang mine(II)	31.64	6.07	0.031	0.232	83.39	16.47	0.08	0.06
93-34	Qiangma mine(I)	12.33	5.05	–	–	70.94	29.06	–	–
93-36	Qiangma mine(II)	9.85	1.63	–	–	85.80	14.20	–	–
93-38	Qiangma mine(II)	34.87	7.11	–	–	83.06	16.94	–	–
93-38[a]	Qiangma mine(II)	35.01	7.17	–	–	83.07	16.93	–	–
GY-1	Guijiayu mine(I)	43.01	20.48	0.008	0.003	67.73	32.26	0.01	0.01
GY-2	Guijiayu mine(II)	37.65	9.97	0.007	0.007	79.04	20.93	0.01	0.01

[a] Denotes duplicate analysis – denotes analysed but not detected

expansion, indicating that they were trapped contemporaneously. Second, CO_2-rich inclusions have the same range of CO_2 homogenisation temperatures as CO_2-H_2O inclusions and they probably represent an unmixed CO_2-rich end-member. Although an H_2O phase is not visible, such CO_2-rich inclusions can contain up to 15 vol% H_2O because the H_2O tends to adhere to the inclusion walls as a thin film (Ramboz et al. 1982; Oslen 1988; Hollister 1988, 1990). These CO_2-rich inclusions should have the same final homogenisation temperatures as the CO_2-H_2O inclusions, but these were not observed due to internal reflection on inclusion margins. Selective entrapment of CO_2-rich composition from a homogeneous one phase CO_2-H_2O fluid following immiscible separation has been suggested by Hollister (1988, 1990) as one of possible mechanism for the formation of CO_2 inclusions. Third, the similar salinity of the primary aqueous inclusions and the water in the CO_2-H_2O inclusions is consistent with fluid immiscibility. The slightly lower homogenisation temperatures of the aqueous inclusions than those of CO_2-H_2O inclusions is also consistent with fluid immiscibility because the CO_2-H_2O inclusions represent mixtures of the two end-members and should have higher homogenisation temperatures. Therefore, fluid immiscibility is a more likely explanation for the various fluid inclusions.

Composition of fluids

Two types of fluids appear to be present in quartz samples associated with gold deposits of the Xiaoqinling district: a CO_2-bearing and a later aqueous fluid. The former is represented by coexisting CO_2-H_2O, CO_2-rich and primary aqueous inclusions described already as having unmixed from a single parent fluid and the latter by secondary aqueous inclusions. The secondary aqueous inclusions in both stage I and II quartz show similar Th_{total} and salinity for each mine, suggesting they were trapped under the same conditions and at the same time after emplacement of stage II veins. This fluid could represent an influx of fluids during the latest stage (III) of vein formation. CO_2-H_2O inclusions are ubiquitously the most abundant in all the studied quartz samples from stages I and II. The quartz examined is intimately intergrown with pyrite which hosts most of the gold. We are, therefore, confident that the CO_2-bearing fluids can be taken as representative of gold associated fluids. Because CO_2-H_2O inclusions are the most abundant, we assume that their mean bulk composition represents the mean composition of the parent vein-forming fluid.

An estimation of bulk composition of CO_2-H_2O inclusions first requires determination of the volume ratios of CO_2 to H_2O phase. According to the methods of Parry (1986) and Brown and Lamb (1989), the mol% CO_2 of CO_2-H_2O inclusions can be determined from laboratory measurements of $Thco_2$, $Tm_{clathrate}$ and Th_{total}. The mol% CO_2 can then be converted to vol% CO_2. The inclusion bulk composition can be determined with the mole or volume percent CO_2, CO_2 density, and salinity using Table 1 of Brown and Lamb (1989). Applying this to our data from the Xiaoqinling district, the CO_2 content of the CO_2-H_2O inclusions from stage I quartz typically falls within the range of 15–30 mol% (20–30 mol% for the Wenyu mine, 18–32 mol% for the Dongchuang mine, 13–24 mol% for the Qiangma mine, 18–30 mol% for the Guijiayu mine). The CO_2 content of CO_2-H_2O inclusions from stage II quartz typically falls within the range of 10–20 mol% (10–19 mol% for the Wenyu mine, 6–20 mol% for the Dongchuang mine, 7–16 mol% for the Qiangma mine, 12–20 mol% for the Guijiayu mine). We believe these to be reasonable estimates for the composition of the original, homogeneous hydrothermal fluids.

For comparison, the data in Table 1 were also used to estimate Xco_2. Although the inclusion gas analyses represent a bulk composition of various inclusions and are contaminated by lesser secondary aqueous inclusions, we still assume that the results reflect the bulk parent fluid compositions to some extent. The Xco_2 values from the four deposits are typically higher than 0.23 in stage I quartz and lower than 0.21 in stage II quartz. These are similar to results from the microthermometric data.

In summary, the parent fluid that deposited the stage I quartz had an approximate salinity of 8.4 equivalent wt.% NaCl and a CO_2 content of 15–30 mol%, whereas the parent fluid for the stage II quartz contained 10–20 mol% CO_2 and had a salinity of 7.1 equivalent wt.% NaCl. In contrast to relatively similar salinities of the CO_2-rich fluids among the four deposits, the salinity of the late aqueous fluids varies notably from one mine to another.

P-T conditions of fluid entrapment

Because the fluid inclusions in stage I and II quartz indicate unmixing during vein precipitation, Th_{total} of the two end-members of the immiscible fluids in the system defines the temperature of entrapment of these fluids. The other inclusions represent mixtures of the two end-members and consequently have higher, but meaningless, homogenisation temperatures. The aqueous and CO_2-rich inclusions distributed in CO_2-H_2O inclusion clusters are considered to represent two end-members of the immiscible fluid and thereby Th_{total} of the primary aqueous inclusions can be considered as the temperature of entrapment. As a result, the temperatures of fluid entrapment of the four deposits are assumed to be 300–370 °C during stage I (Wenyu mine, 320–400 °C; Dongchuang mine, 275–360 °C; Qiangma mine, 295–335 °C; Guijiayu mine, 325–380 °C) and 250–320 °C during stage II (Wenyu mine, 290–335 °C; Dongchuang mine, 240–320 °C; Qiangma mine, 245–290 °C; Guijiayu mine, 300–330 °C).

Based on the calculated fluid composition and estimated fluid trapping temperatures, several immiscibility *P-T-X* curves for the system H_2O-CO_2-NaCl (Bowers and Helgeson 1983) were chosen to estimate the trapping pressures of the fluids. We assume maximum pressures did not exceed about 2 kbar based on depth of emplacement estimates of the Yanshanian granites (Luan et al. 1991) that are interpreted related to the vein-forming events. The CO_2-H_2O inclusions in stage I quartz plot around the H_2O-CO_2-6 wt.% NaCl solvus at 2 kbar for all deposits (Fig. 5A), although the field for the Dongchuang mine is slightly lower in temperature than the three other fields. In fact, the average salinities of CO_2-H_2O inclusions in stage I quartz are 7.1 to 9.2 equivalent wt.% NaCl for the four deposits. The addition of a few percent more salinity to the 6 wt.% system will raise the solvus to higher temperatures. The trapping pressures will be, therefore, slightly higher than 2.0 kbar. We select 2.2 kbar as the approximate trapping pressures of fluids during stage I veining for the four deposits, although there might be some minor difference among the four deposits. Most CO_2-H_2O inclusions in stage II quartz plot between the H_2O-CO_2-6 wt.% NaCl solvus at 1 kbar and that at 2 kbar (Fig. 5B). Because the salinities of CO_2-H_2O inclusions in stage II quartz are generally slightly higher than 6 equivalent wt.% NaCl (5.7 to 8.4 equivalent wt.%), we assume the appropriate position to be slightly higher in temperature and estimate 1.6 kbar as the trapping pressure for stage II fluids.

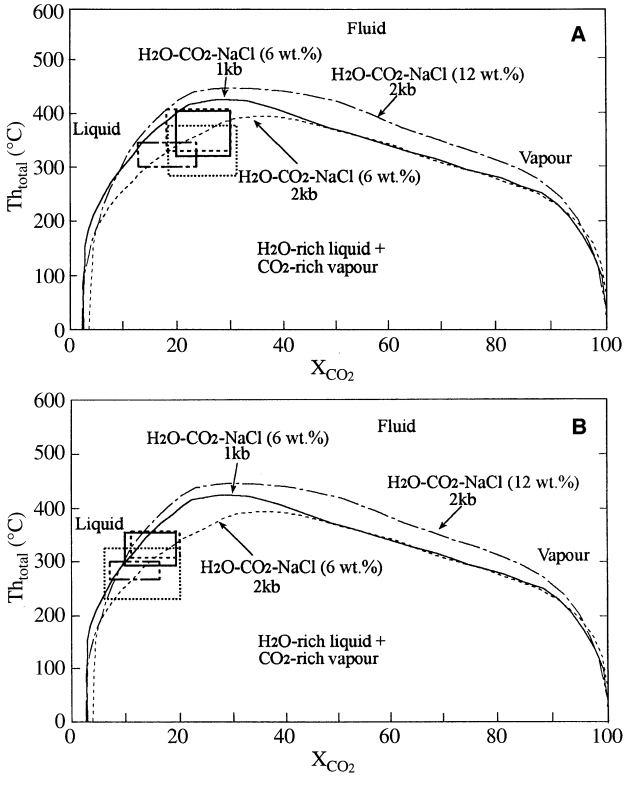

Fig. 5 A, B Total homogenisation temperature versus calculated mol fraction of CO_2 for CO_2-H_2O inclusions. Solvi from Bowers and Helgeson (1983) **A** stage I, **B** stage II, *Solid-lined box*, Wenyu mine; *dot-lined box*, Dongchuang mine; *dash and dot-lined box*, Qiangma mine; *dash-lined box*, Guijiayu mine

Implications for source of the fluids

Low-salinity CO_2-rich hydrothermal fluids have been implicated for the genesis of the gold mineralisation in the Xiaoqinling district, a fluid type which is also typical of many Archean and Phanerozoic lode gold deposits (Bohlke and Kistler 1986; Robert and Kelly 1987; Kerrich 1989; Naden and Shepherd 1989). The main hypotheses on the fluid source for those types of deposits suggest igneous source (Burrows et al.1986; Burrows and Spooner 1987; Cameron and Hattori 1987) or metamorphic components (Kerrich and Fyfe 1981; Goldfarb et al. 1988; Kerrich 1989).

In the Xiaoqinling district, regional metamorphism took place at 2600-2300 Ma (Lin et al. 1989) and migmatisation between 2000 and 900 Ma (Hu and Lin 1988). There was no metamorphism immediately before or during late Mesozoic gold mineralisation. Therefore, the CO_2-rich fluids are presumably not derived from a metamorphic source. The fluids that deposited the gold-bearing veins are most likely igneous in origin. The close temporal and spatial association between ore-bearing veins and the Yanshanian granitoids suggests that deep-crustal granitic devolatilisation would have generated the mineralising fluids.

Downward-percolating meteoric water is commonly reported to be a salinity, aqueous fluid (Garba and Akande 1992). The late aqueous fluid in stage II veins varies from low salinity (Wenyu mine, 3.1–6.7 equivalent wt.% NaCl; Qiangma mine, 4.0–10.1 equivalent wt.% NaCl; Guijiayu mine, 1.4–5.6 equivalent wt% NaCl) to moderate salinity (Dongchuang mine, 10.1 to 13.5 equivalent wt% NaCl). Despite the moderate salinities at the Dongchuang mine, fluid in inclusions in late fractures in both stage I and stage II veins can be best explained by an influx of local meteoric water.

The most remarkable feature of the ore-forming fluids in all four studied deposits of the Xiaoqinling district is the uniformity in fluid evolution, and fluid composition. This favours introduction of vein-forming fluids from a single source area at all four deposits. The differently oriented veins within Xiaoqinling district do not vary in fluid composition. Therefore, all veins probably formed during a single, large hydrothermal episode.

Fluid evolution and gold deposition

Fluid inclusions in both stage I and II quartz show evidence of fluid immiscibility. However, stage I veins only contain minor gold and pyrite. Thus we cannot relate gold deposition solely to fluid immiscibility.

The primary fluid inclusions in quartz from stage I and II evolve record an evolution to lower fluid P, T, and Xco_2. Because inclusions in the studied quartz are closely associated with sulphide grains, the inclusions are believed to contain fluid responsible for precipitation of both sulphides and quartz. Gold occurs as fracture-fillings accompanying anhedral chalcopyrite and galena, or as inclusions in fine-grained pyrite, indicating gold deposition is contemporaneous with sulphide precipitation. The low content of gold in stage III veins precludes gold introduction into stage II veins during stage III hydrothermal events. Therefore, gold is interpreted as being deposited during stage II vein formation. The pressure and temperature of CO_2-H_2O inclusions in stage II quartz are somewhat lower than that of stage I quartz. Perhaps some combination of fluid immiscibility and decreases in pressure and temperature between stage I and II together are critical to gold deposition during stage II veining.

Acknowledgements Financial support for the research was provided by the President Foundation of Chinese Academy of Sciences. We specifically thank E Molan, Jin Chengwei, Xie Yihan and Fan Hongrui for valuable comments in developing and clarifying the paper and for support of field survey. The assistance of Wang Y. with the gas analyses is gratefully acknowledged. Insightful comments by Richard J. Goldfarb and Tony Christie substantially improved presentation of the manuscript. An early version of the manuscript benefited from constructive criticism by two anonymous reviewers.

References

Bohlke JK, Kistler RW (1986) Rb-Sr, K-Ar, and stable isotope evidence for ages and sources of fluid components of gold-bearing quartz veins in the northern Sierra Nevada foothills metamorphic belt, California. Econ Geol 81: 296–322

Bodnar RJ (1993) Revised equation and table for determining the freezing point depression of H_2O-NaCl solutions. Geochim Cosmochim Acta 57: 683–684

Bowers TS, Helgeson HC (1983) Calculations of the thermodynamic consequences of nonideal mixing in the system H_2O-CO_2-NaCl on relations in geologic systems: equation of state for CO_2-H_2O-NaCl fluids at high pressures and temperatures. Geochim Cosmochim Acta 47: 1247–1275

Brown PE, Lamb WM (1989) P-V-T properties of fluid in the system $CO_2 \pm H_2O \pm$ NaCl: New graphical presentations and implication for fluid inclusion studies. Geochim Cosmochim Acta 53: 1209–1221

Burrows DR, Wood PC, Spooner ETC (1986) Carbon isotope evidence for a magmatic origin for Archean gold-quartz vein ore deposits. Nature 321: 851–854

Burrows DR, Spooner ETC (1987) Generation of a magmatic H_2O-CO_2 fluid enriched in Mo, Au, and W within an Archean sodic granodiorite stack, Mink Lake, Northwestern Ontario. Econ Geol 82: 1931–1957

Cameron EM, Hattori K (1987) Archean gold mineralisation and oxidized hydrothermal fluids. Econ Geol 82: 1177–1191

Chao Y (1989) The metallogenetic epoch of the Xiaoqinling gold deposits. Geology of Shaanxi, 7: 52–55 (in Chinese)

Collins PLF (1979) Gas hydrates in CO_2-bearing fluid inclusions and the use of freezing data for estimation of salinity. Econ Geol 74: 1435–1444

Fang Y (1985a) Native gold and its fineness in gold-bearing veins in Xiaoqinling district. Geology of Henan 3: 27–33 (in Chinese)

(1985b) The gold content of pyrite in gold-bearing veins in Xiaoqinling district. J Chengdu Inst. Geol 12 (2): 1–12 (in Chinese)

Garba I, Akande SL (1992) The origin and significance of non-aqueous CO_2 fluid inclusions in the auriferous veins of Bin Yauri, north-western Nigeria: Mineralium Deposita 27: 249–255

Goldfarb RJ, Leach DL, Pickthorn WJ, Paterson CJ (1988) Origin of lode-gold deposits of the Juneau gold belt, southeastern Alaska. Geology 16: 440–443

Hollister LS (1988) On the origin of CO_2-rich fluid inclusions in migmatites. J Metam Geol 16: 467–474

Hollister LS (1990) Enrichment of CO_2 in fluid inclusions in quartz by removal of H_2O during crystal-plastic deformation. J Struct Geol 12: 895–901

Hu S, Lin Q (1988) The geology and metallogeny of the amalgamation zone between ancient north China Plate and south China Plate. Nanjing University Publishing House (in Chinese)

Ji J (1991) A hydrogen and oxygen isotope and fluid inclusion study of gold deposits in western Xiaoqinling. Mineral Dep 10: 283–287 (in Chinese)

Kerrich R, Fyfe WS (1981) The gold-carbonate association: source of CO_2 and CO_2 fixation reactions in Archean lode deposits. Chem Geol 33: 265–294

Kerrich R (1989) Archean gold: Relation to granulite formation or felsic intrusions? Geology 17: 1011–1015

Li B, Zhou Z, Xie Y, Xie Z, Wang Y, Li R (1989) Characters of fluid inclusion and ore genesis of Xiaoqinling gold deposits. Proc Int Symp Gold Geology and Exploration, p 513–515 (in Chinese)

Li S, Chu L, Su Z, Huang J, Wang X, Yue Z (1996) Geology and metallogenic prognosis of gold deposits in Xiaoqinling district, China. Geological Press, Beijing (in Chinese)

Lin B, Tao T, Li G, Bai Q, Zhang Z (1989) A research on the main gold-bearing strata, Xiaoqinling district along the border area of Henan and Shaanxi provinces. In: Contributions to the project of regional metallogenetic conditions of main gold deposit types in China, III. Xiaoqinling area in Henan and Shaanxi provinces, p1–46. Geological Press, Beijing (in Chinese)

Luan S, Chen S, Cao D, Fang Y (1985) Geochemistry of gold deposits in Xiaoqinling district. Minerals Rocks 5 (2): 118p (in Chinese)

Luan S, Chen S, Cao D, Fang Y (1991) Characteristics of the deep-seated gold mineralisation and its evaluational criteria in Xiaoqinling area. Press of Chengdu University of Science Technology (in Chinese)

Naden J, Shepherd TJ (1989) Role of methane and carbon dioxide in gold deposition. Nature 342: 793–795

Oslen SN (1988) High density CO_2 inclusions in the Colorado Front range. Contrib Mineral Petrol 100: 226–235

Parry WT (1986) Estimation of Xco_2, P, and fluid inclusion volume from fluid inclusion temperature measurements in the system NaCl-CO_2-H_2O. Econ Geol 81: 1009–1013

Ramboz C, Pichavant M, Weisbrod A, (1982) Fluid immiscibility in natural processes: use and misuse of fluid inclusion data. II. Intepretation of fluid inclusion data in term of immiscibility. Chem Geol 37: 29–48

Robert F, Kelly WC (1987) Ore-forming fluids in Archean gold-bearing quartz veins at the Sigma Mine, Abitibi Greenstone Belt, Quebec, Canada. Econ Geol 82: 1464–1482

Roedder E (1984) Fluid inclusions. Mineralogical Society of America, Reviews in Mineralogy 12: p 644

Shepherd TJ, Rankin AH, Alderton DHM (1985) A practical guide to fluid inclusion studies. Blackie pp 239

Xie Y, Jin C, Zhao R, Fan H, Wang Y, Tian G (1996) Fluid evolution of fluid and gold metallogenesis in Xiaoqinling district. In: Advances of gold deposits researches in China 1: 351–365. Seismological Press, Beijing (in Chinese)